AUTOMATIC DETECTION AND MAPPING OF IRRIGATION SYSTEM FAILURES USING REMOTELY SENSED CANOPY TEMPERATURE AND IMAGE PROCESSING

V. Alchanatis, Y. Cohen, M. Sprinstin and A. Cohen

Department of Sensing, Information and Mechanization Systems.
Institute of Agricultural Engineering, Agricultural Research Organization (ARO)
Volcani Center, P.O. Box 6, Bet Dagan, 50250, Israel.

A. Dag and I. Zipori

Agricultural Research Organization (ARO),Volcani Center
Gilat Research Center, Israel.

A. Naor

The Golan Research Institute
University of Haifa, Israel.

ABSTRACT

Today there is no systematic way to identify and locate failures of irrigation systems mainly because of the labor costs associated with locating the failures. The general aim of this study was to develop an airborne thermal imaging system for semi - automatic monitoring and mapping of irrigation system failures, specifically, of leaks and clogs.

Detection of real faults was attempted: a preliminary algorithm was developed to identify suspicious areas (suspected faults) based on the distribution of canopy temperature. To examine the accuracy and reliability of the algorithm five sites were selected with olive groves (Gshur and Revivim), vines (Lachish), palm dates (Kalia and Almog) and almonds (Lavi). This paper presents the results obtained from two sites with olive groves and one site with vines. Each site covered approximately 100 hectares. To access the accuracy and reliability of the algorithm, it was combined with the estimated potential savings in labor. The results indicated the following: 1. according to the map produced by the algorithm, 14-20% of the area has to be scanned, which corresponds to a 60% saving of the time needed to scan the whole area 2. The automatically detected suspicious areas contain at least 80% of the visible faults. 3. Most of the area that is detected for scan will not contain visible faults. However, it was found that in 70% of the locations suspected for leaks the trees indeed received excess water relative to their surroundings, and in 90% of the locations suspected for clogs the trees suffered from lack of water relative to their surroundings. That is, the map produced by the developed algorithm allows to save about 60% of the scan time,

detects about 80% of the visible leaks, and detects leaks and clogs that are not visible with a reliability of 70% and 90% respectively.

Despite the benefits of the semi - automatic algorithm it requires input of four empirical parameters that can change its performance: minimum distance between pixels to create the histogram, size of pixels clusters associated with leaks and clogs, parameters associated with image enhancement (erosion) and allowed tolerance in estimating the location of the leak or clog. The algorithm has not yet been tested on palm dates and we intend to test it in the future.

Keywords: olives, table grapes, leaks, clogs, tree specific management

INTRODUCTION

Malfunctions are usually associated with improper maintenance or operation of irrigation system (e.g. physical damages caused by vehicles and/or animals or use of low-quality water) and appear as leaks and clogs in irrigation lines having both direct and indirect effects on within-field yield variability. Directly, the water lost by surface or sub-surface flow to unwanted areas in the field/orchard vicinity or by infiltrating to ground water, while indirectly it can cause a significant decrease in yield quality and quantity as a result of inadequate use of already invested resources. Therefore, frequent monitoring of on-site irrigation system is an important task that farmers undertake. Though important, this task is tedious, costly, labour-intensive and generally uneasy to be implemented on regular basis. For that reason, the employment of a technology that improves the efficiency of large-scale monitoring of irrigation malfunctions could benefit to economic profitability of agricultural systems. Providing that either clog or leak could be associated with a change in the amount of water received by the plant (as over- or under-irrigation), evaluation of crop water status could be a practical way to detect within field/orchard spots where either malfunction could be speculated. There are several direct and indirect indicators of crop water status (i.e. water stress) have been presented and practically utilized by farmers in irrigation scheduling (e.g. soil moisture availability, stem water potential, stomatal conductance, assimilation rate and tree transpiration rate). Though well studied (Selles and Berger, 1990; Ramos et al., 1994; Bonany et al., 2000; Marsal et al., 2002; Naor and Cohen, 2003; Naor, 2006; 2008), those indicators are mostly lack spatial dimension and thus cannot be practically used in malfunctions monitoring. Contrary the fact that any change in water amounts received by plants will alter stomata opening and thus transpiration cooling (Jones, 1992) has triggered recognition of canopy temperature to be an indicator of plant water status (Tanner, 1963; Gates, 1964; Idso et al., 1978; Fuchs et al., 1987).

The availability of non-invasive technology for measuring crop surface temperature either by closed range thermal infrared (TIR) thermometers (e.g. Jones, 1999) or by thermal imaging systems carried by ground-based (Moller et al., 2007), airborne (e.g. Meron et al., 2003, Alchanatis et al., 2010) or spaceborne (Sprintsin et al., 2011) platforms provides a theoretically sound and practically

useful way to detect and map the inadequately irrigated areas quantitatively or/and qualitatively. Mapping absolute (in terms of water potential, Alchanatis et al., 2010) and relative (by means of water stress index, Idso et al., 1978; Moller et al., 2007) plant water status might provide the growers with information about extreme conditions related to malfunctioning of the irrigation system or variable irrigation efficiencies (e.g., Meron et al., 2003; Naor, 2006). It should be noted, however, that despite the variety of techniques and platforms, the question of reliability of each one of them to farm management in terms of cost and spatial resolution remains open. While the largest pixel size of an imagery obtained by ground-based observations provides an easiest way of separation between malfunction of different spatial extent, the low observation height and hence the small field of view of such a system is questioning its usefulness in spatial monitoring. On the other hand, the spatial resolution of currently available satellite TIR imagery (i.e. 60-1000m2) in most of the cases could not be used in assessing the within-field variability of crop water status and its employment in precision agriculture is questionable as well.

Alternatively, the appropriateness of airborne thermal imagery in water stress assessment and site-specific irrigation has been successfully presented for a wide variety of crops (i.e. Sepulcre-Canto et al., 2006; Alchanatis et al., 2010; Gonzalez-Dugo et al., 2011). The imagery, obtained by airborne platforms has a spatial resolution that from one hand is high enough to produce within-field maps of irrigation levels and from another, the field of view that is large enough to be useful at field and even at small regional scale. Such a combination of technical characteristics makes this imagery to be almost a unique tool for spatial assessment of irrigation related phenomena.

This paper presents an attempt to evaluate the applicability of airborne thermal imagery for semi-automatic detection and mapping of the malfunctions in irrigation lines as a first step in developing a technology for continuous monitoring and maintenance of irrigation system. Our specific objectives were: (a) to develop and test an algorithm for semi-automatic processing of airborne TIR imagery for detection and mapping of several types of irrigation malfunction and (b) to characterize the practical issues to be addressed in detection of irrigation malfunctions by means of remote sensing observations.

MATERIALS AND METHODS

Field plots:

The study has been conducted at three different geographical regions: Commercial vine fields of mature (over 8 years) plantations of table grapes located at the costal desert in southern Israel (31.56 N 34.86 E; ~240m ASL; Lakhish farm). The grapes variety was Thompson, planted at 3x1.5m intervals and irrigated by a drip system with one line per row, according to the commercial irrigation practice. A total area of about 100 ha of vineyards was used in this study. Commercial olive groves were located near Kibutz Revivim (31.052 N 34.71 E, Kibutz Revivim, about 100 ha) and near Kibutz Gshur (32.82 N 35.72 E Kibutz Gshur about 100 ha). Several olive varieties were included, mainly

Barnea, Suri and Picual. The interval between trees ranged from 2-3 m and the interval between the rows was about 3 m.

Image acquisition:

Thermal images (TIR) were acquired with an uncooled thermal infrared camera (IR-TCM640, Jenoptics Inc., Germany). The camera has a microbolometer sensor operating in the 8-14μm spectral range with thermal resolution of 0.05°K and temperature accuracy of about 1°K. The camera has a resolution of 640x480 pixels. The flight height was approximately 500 m above the ground, resulting to 0.35 m per pixel on the ground. Nadir images were acquired under clear sky conditions during the midday hours (12:00-3:00 PM) when the stomata opening has been assumed to reach its potential maximum under amply water supply. RGB (red-green-blue) images were also acquired at the same hours as TIR during an additional overpass with a ground resolution of 0.05 m per pixel. The TIR and RGB images were co-registered and geo-referenced to the new Israeli coordinates grid. They were processed using Matlab R13 software (Mathworks Inc., Natick, MA, USA) to map the canopy temperature.

Ground truth:

Irrigation malfunctions were recorded in two ways. The whole area was scouted on foot, and all the visible failures were marked using handheld GPS receivers with GIS software (ArcPad, ESRI). Each location was geo-tagged, labeled as 'leak' or 'clog', a picture was taken and archived. The irrigation system was activated during the scouting, in order to be able to visually recognize malfunctions. In addition to visual inspection, field measurements of Stem Water Potential (SWP) of vines and olive trees were conducted. The locations for SWP measurements were selected after analyzing the thermal images, and included suspicious points, were visual inspection had not revealed an abnormal situation. Two trees were selected per location for pairwise comparison: the suspicious tree, and a neighboring normally appearing tree. SWP was measured on pre-wrapped, shaded leaves after two hours of on-plant equilibration, with ARIMAD-7000 pressure chamber (MRC Ltd., Israel) a day after image acquisition.

Meteorological conditions:

Air temperature, relative humidity, global radiation and wind speed were measured by a meteorological station located within the experimental plot. The sampling interval was 10 s (excluding wind which was sampled every 1 s), and 1-min averages were recorded by a data logger (Campbell Scientific, Logan, UT, USA). Meteorological conditions were measured throughout all hours of data collection (image acquisition and measurement of stem water potential).

Processing of thermal images:

Image processing was based on analysis of the temperature histogram of the field. Pixels of soil were masked out, assuming that their temperature is higher than 5 degrees above air temperature. The rest of the pixels were assumed to represent canopy.

Trees edges contain potentially mixed pixels (soil and leaves), whose temperature does not represent the canopy temperature. In order to avoid mixed pixels, after soil was masked out, morphological erosion was performed to omit potentially mixed pixels. Figure 1 shows the canopy histogram before and after the erosion.

The histogram of the canopy pixels was then used to detect temperature anomalies. Assuming that canopy temperature distribution is normal (Gaussian), pixels that lay outside a number of standard deviations from the mean of the population were labelled as anomalies. Pixels cooler than the average were treated as suspicious for leak, and pixels warmer than the average were treated as suspicious for clogging.

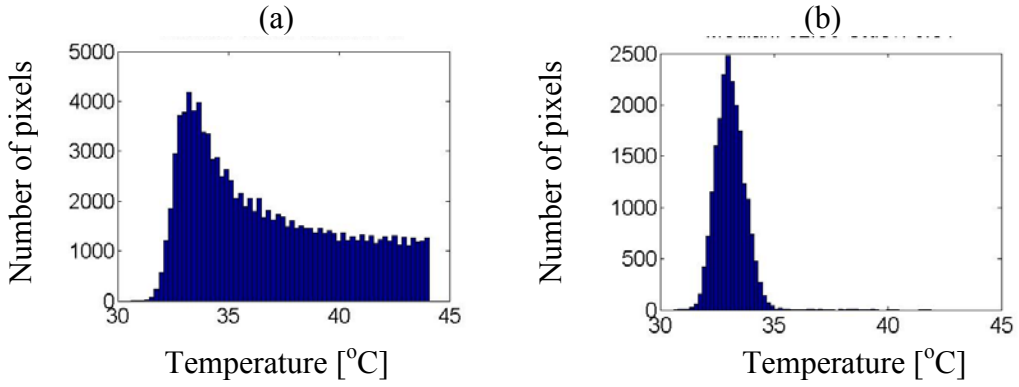

Figure 1. Histogram of canopy temperature: (a) before erosion, (b) after erosion

Performance evaluation

Detection accuracy and errors were evaluated by comparing the scouting results with the automatically generated suspicious points. A suspicious point for leak or clog (from image analysis) was considered to be correctly detected if a leak or a clog was manually marked within a radius of 10 m from the suspicious point. In addition to that, if no visible signs were noted around the suspicious point, and a SWP measurement was performed, then a difference of 2Mpa between the suspected tree and its surroundings was also denoted as a success.

RESULT AND DISCUSSION

Figure 2 shows a sample map of the scouting data from the olive groves in Gshur. The green border lines delineate the irrigation blocks. Each irrigation

block consists of several varieties, with a number of rows of each variety. Each dot represents a location where an event was recorded. The GIS geo-database includes the type of malfunction, the severity level and an image of the area where the malfunction was detected. In each irrigation block, tens of abnormal things were observed. These points serve as the gold standard for the automatic detection of the faults.

Figure 2. Map of the data acquired from scouting. Each circle represents a recorded event, and has a record with meta-data in the geo-database.

The image processing algorithms described in the previous section produced maps of locations suspected for faults (figure 3). Each location with a temperature higher than two standard deviations from the mean temperature (considering each irrigation block individually) was marked with red color and was suspected as a

clog. Each location with a temperature lower than two standard deviations from the block mean temperature was marked black and was suspected as a leak. For each irrigation block, a list of the suspicious points coordinates was automatically generated. This list can serve as an input to navigation software that directs the farmer to inspect the suspicious locations.

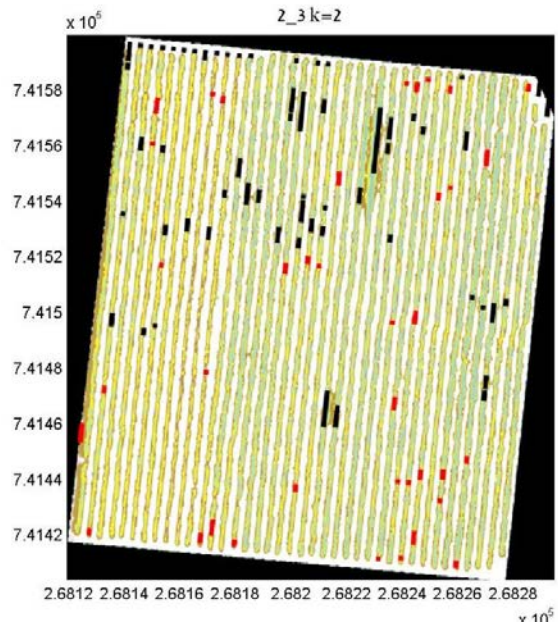

Index	x	y	Type
1	268135.5	741497.6	Low
2	268139.7	741535.4	Low
3	268141.5	741588.6	Low
4	268141.8	741593.8	Low
5	268146	741595.9	Low
6	268146	741560.9	Low
7	268147.1	741493	Low
8	268149.9	741595.6	Low
9	268151.3	741495.1	Low
10	268154.1	741595.2	Low
11	268154.1	741558.8	Low
12	268154.8	741529.8	Low
13	268157.9	741594.9	Low
14	268161.8	741594.5	Low
15	268162.8	741531.5	Low
16	268165.6	741594.2	Low

Figure 3. Map with the locations of suspicious points. Red points represent locations suspected for clog, and black points represent locations suspected for leak. A table with the geographical coordinates of the suspected points is also generated and show next to the map.

Detection accuracy was evaluated for the "leaks" (anomalies with lower temperature) for all the three plots in two different occasions. The irrigation malfunctions were divided into three severity levels, high low and intermediate. The accuracy and the misses of the automatic algorithm to detect these leaks are shown in table 1. The algorithm performance was evaluated with three different threshold values for anomalies: deviation of 1, 1.5 and 2 standard deviations from the block mean temperature.

Referring to the threshold associated with anomaly detection, the results show that a lower level of deviation yields to better performance: higher correct detection rate (accuracy) and lower false detection rate (misses) (table 1). When a value of one standard deviation is used, the highest accuracy is obtained.

Figure 4 summarizes the detection accuracy of the different malfunction severity levels when the anomaly detection threshold is set to one standard deviation from the mean canopy temperature of the plot. The severe malfunctions are detected with very high accuracy: over 85% for grapes and 100% for all olives groves. In grapes, in the earlier date the accuracy was slightly higher than the date later in the season. For olives, 100% correct detection was maintained across the season and the geographical region.

Table 1. Detection accuracy (correct) and missed points (false) of the three crops in two dates, detailed according to different malfunction severity levels and according to three anomaly detection levels.

Anomaly detection level (number of standard deviations from the mean)									
1		1.5		2					
False	**Correct**	**False**	**Correct**	**False**	**Correct**	**No of samples (n)**	**Malfunction Severity**	**Date**	**Crop**
	90%	30%	70%	50%	50%	10	High	10.6.12	**Vineyards – Lachish area)**
0%	100%	100%	0%	100%	0%	1	Low		
42%	58%	65%	35%	86%	14%	66	Unkn.		
38%	62%	61%	39%	82%	18%	77	All		
15%	85%	51%	49%	83%	17%	47	High	19.8.12	
26%	74%	52%	48%	72%	28%	46	Interm.		
29%	71%	53%	47%	81%	19%	59	Low		
16%	84%	32%	68%	68%	32%	31	Unkn.		
22%	78%	49%	51%	77%	23%	183	All		
0%	100%	0%	100%	0%	100%	2	High	24.6.12	**Olives – (Gshur area)**
0%	100%	50%	50%	100%	0%	2	Interm.		
40%	60%	60%	40%	80%	20%	5	Low		
17%	83%	50%	50%	73%	27%	30	Unkn.		
18%	82%	49%	51%	72%	28%	39	All		
0%	100%	29%	71%	29%	71%	7	High	26.8.12	
19%	81%	43%	57%	67%	33%	21	Interm.		
36%	64%	69%	31%	90%	10%	39	Low		
0%	100%	0%	100%	100%	0%	1	Unkn.		
26%	74%	56%	44%	76%	24%	68	All		
0%	100%	29%	71%	57%	43%	7	High	17.6.12	**Olives – (Revivim area)**
0%	100%	100%	0%	100%	0%	1	Interm.		
0%	100%	50%	50%	100%	0%	2	Low		
16%	84%	47%	53%	74%	26%	137	Unkn.		
15%	85%	46%	54%	74%	26%	147	All		
0%	100%	20%	80%	25%	75%	20	High	12.8.12	
13%	88%	50%	50%	69%	31%	16	Interm.		
21%	79%	58%	42%	82%	18%	38	Low		
13%	87%	36%	64%	59%	41%	83	Unkn.		
13%	**87%**	**41%**	**59%**	**61%**	**39%**	**157**	**All**		

Detection of intermediate severity leaks was less accurate, and detection of low severity leaks was even less accurate. Nevertheless, for the olives, the accuracy was still maintained high (more than 80% for intermediate severity, and between 60-85% for the low severity leaks. Comparing the results of the vines with the results of the olives, the detection accuracy in the olives groves is generally higher than that of the vines, in almost all the cases. This difference may be explained by the different irrigation regime of the two crops. Table grapes vines are irrigated in excess, in order to ensure high yield by weight, while olive trees are maintained in controlled deficit in order to balance the water and olive accumulation in the fruits. As a consequence, excessive water availability caused by leaks do not change significantly the water status of the vines, since they are already irrigated in excess. On the other hand, olive trees that are maintained in deficit, are directly affected by excessive water resulting to higher evapotranspiration rates.

According to the map produced by the algorithm, 14-20% of the area has to be scanned, which corresponds to a 60% saving of the time needed to scan the whole area. However, it was found that in 70% of the locations suspected for leaks the trees indeed received excess water relative to their surroundings, and in 90% of the locations suspected for clogs the trees suffered from lack of water relative to their surroundings. That is, the map produced by the developed algorithm allows to save about 60% of the scan time, detects about 80% of the visible leaks, and detects leaks and clogs that are not visible with a reliability of 70% and 90% respectively. Automatically detected suspicious areas contain at least 80% of the visible faults. 3. Most of the area that is detected for scan will not contain visible faults. However, it was found that in 70% of the locations suspected for leaks the trees indeed received excess water relative to their surroundings, and in 90% of the locations suspected for clogs the trees suffered from lack of water relative to their surroundings. That is, the map produced by the developed algorithm allows to save about 60% of the scan time, detects about 80% of the visible leaks, and detects leaks and clogs that are not visible with a reliability of 70% and 90% respectively.

Despite the benefits of the semi - automatic algorithm it requires input of four empirical parameters that can change its performance: minimum distance between pixels to create the histogram, size of pixels clusters associated with leaks and clogs, parameters associated with image enhancement (erosion) and allowed tolerance in estimating the location of the leak or clog. The algorithm has not yet been tested on palm dates and we intend to test it in the future.

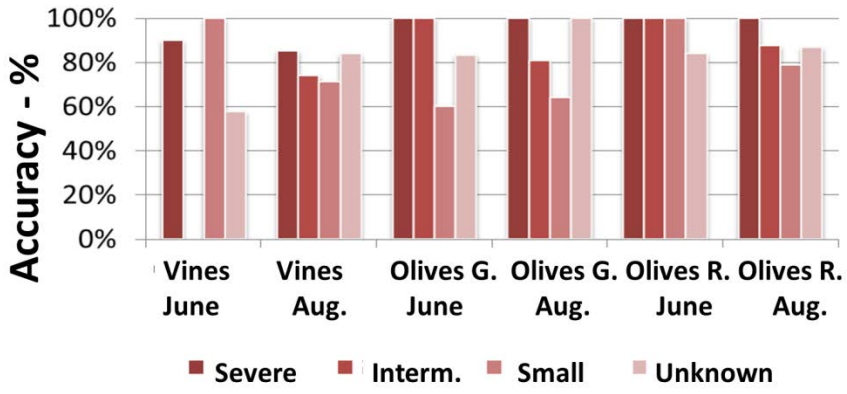

Figure 4. Summary of leaks detection accuracy when anomalies are considered as temperature deviations of one standard deviation from the mean canopy temperature of the plot.

CONCLUSIONS

The results of this study showed that remotely sensed thermal images can be used to detect irrigation malfunctions. Specifically, severe leaks are detected with very high accuracy, while less severe malfunctions exhibit less accurate detection. For its assimilation the cost effectiveness of the thermal-based irrigation management should be examined in commercial scales. Future study should focus on the applicability of this approach with farmers.

ACKNOWLEDGEMENTS

This research was supported by grant No. 458-0521-12 from the Chief Scientist of the Israeli Ministry of Agriculture. We would like to thank the farmers and extension leaders for their time they invested to hand us the information on the plots.

REFERENCES

Alchanatis, V., Cohen, Y., Cohen, S., Moller, M., Sprinstin, M., Meron, M., Tsipris, J., Saranga, Y., and Sela, E., (2010). Evaluation of different approaches for estimating and mapping crop water status in cotton with thermal imaging. Precision Agriculture, 11, 27–41. DOI 10.1007/s11119-009-9111-7.

Bonany, J., Camps, F. and Salva, J., (2000). Relationships between trunk diameter fluctuations, stem water potential and fruit growth rate in potted adult apple trees. Acta Hort., 511, 43-49.

Fuchs, M., Cohen, Y., and Moreshet, S., (1987). Determining transpiration from meteorological data and crop characteristics for irrigation management. Irrigation Science, 8, 91-99.

Gates, D. M., (1964). Leaf temperature and transpiration. Agronomy Journal, 56, 273–277.

Gonzalez-Dugo, V., Zarco-Tejada, P., Berni, J.A.J., Suarez, L., Goldhamer, D., and Fereres, E., (2011). Almond tree canopy temperature reveals intra-crown

variability that is water stress-dependent. Agricultural and Forest Meteorology 154– 155, 156– 165.

Idso, S.B., Reginato., R.J., and Jackson, R.D., (1978), An equation for potential evaporation from soil, water, and crop surfaces adaptable to use by remote sensing. Geophysical Research Letters, 4, 187-188.

Jones, H. G., (1992). Plants and microclimate (2nd ed., pp. 231–236). Cambridge, UK: Cambridge University Press.

Jones, H.G., (1999). Use of infrared thermometry for estimation of stomatal conductance as a possible aid for irrigation scheduling. Agric. For. Meteor., 95, 139-149.

Marsal, J., Mata, M., Arbonés, A., Rufat, J., and Girona, J., (2002). Water stress limits for vegetative and reproductive growth of 'Bartlett' pears. Acta Hort., 596, 659-664.

Meron, M., Tsipris, J., & Charitt, D., (2003). Remote mapping of crop water status to assess spatial variability of crop stress. In J. V. Stafford & A. Werner (Eds.), Precision agriculture '03: Proceedings of the 4th European conference on precision agriculture (pp. 405–410). Wageningen, The Netherlands: Wageningen Academic Publishers.

Moller, M., Alchanatis, V., Cohen, Y., Meron, M., Tsipris, J., Naor, A., Ostrovsky, V., Sprintsin, M., and Cohen, S., (2007). Use of thermal and visible imaginary for estimating crop water status of irrigated grapevine. J. Exp. Bot., 58(4), 827-838. doi:10.1093/jxb/erl115.

Naor, A., (2006). Irrigation Scheduling and Evaluation of Tree Water Status in Deciduous Orchards. Horticultural Reviews, 32, 111-165.

Naor, A., (2008). Water Stress Assessment for Irrigation Scheduling of Deciduous Trees, Proc. Vth IS on Irrigation of Hort. Crops, Eds.: I. Goodwin and M.G. O'Connell, Acta Hort.792, ISHS.

Naor, A., and Cohen, S., (2003). The sensitivity and variability of maximum trunk shrinkage, midday stem water potential, and transpiration rate in response to withholding of irrigation in field-grown apple trees. HortScience, 38, 547-551.

Ramos, D.E., Weinbaum, S.A., Shackel, K.A., Schwankle, L.J., Mitcham, E.J., Mitchell, F.G., Snyder, R.G., Mayer, G., and McGourty, G., (1994). Influence of tree water status and canopy position on fruit size and quality of Bartlet pears. Acta Hort., 367, 192-200.

Selles, G., and Berger, A., (1990). Physiological indicators of plant water status as criteria for irrigation scheduling. Acta Hort., 278, 87-100.

Sepulcre-Canto, G., Zacro-Tejada, P.J., Jimenez-Munoz, J.C., Sobrino, J.A., de Miguel, E. and Villalobos, F.J., (2006). Detection of water stress in an olive orchard with thermal remote sensing imagery. Agric. For. Meteor. 136, 31-44.

Sprintsin, M., Chen, J.M., and Czurylowicz, P., 2011. Combining land surface temperature and shortwave infrared reflectance for early detection of mountain pine beetle infestations in western Canada, Journal of Applied Remote Sensing, 5, 053566/1-053566/13.

Tanner, C.B., (1963). Plant temperature. Agronomy Journal, 55, 210-211.